

# Bioconjugated quantum dots for multiplexed and quantitative immunohistochemistry

Yun Xing<sup>1</sup>, Qaiser Chaudry<sup>2</sup>, Christopher Shen<sup>1</sup>, Koon Yin Kong<sup>2</sup>, Haiyen E Zhou<sup>3</sup>, Leland W Chung<sup>3</sup>, John A Petros<sup>3,4</sup>, Ruth M O'Regan<sup>5</sup>, Maksym V Yezhelyev<sup>5</sup>, Jonathan W Simons<sup>1,5</sup>, May D Wang<sup>1,2,5</sup> & Shuming Nie<sup>1,5</sup>

<sup>1</sup>Department of Biomedical Engineering, Emory University and Georgia Institute of Technology, 101 Woodruff Circle Suite 1001, Atlanta, Georgia 30322, USA. <sup>2</sup>Department of Electrical and Computer Engineering, Georgia Institute of Technology, Atlanta, Georgia 30332, USA. <sup>3</sup>Department of Urology, Emory University School of Medicine, Atlanta, Georgia 30322, USA. <sup>4</sup>Veteran Affairs Medical Center, Atlanta, Georgia, 30333, USA. <sup>5</sup>Department of Hematology and Oncology and the Winship Cancer Institute, Emory University School of Medicine, Atlanta, Georgia 30322, USA. Correspondence should be addressed to M.D.W. (maywang@bme.gatech.edu) or S.N. (snie@emory.edu).

Published online 3 May 2007; doi:10.1038/nprot.2007.107

**Bioconjugated quantum dots (QDs) provide a new class of biological labels for evaluating biomolecular signatures (biomarkers) on intact cells and tissue specimens. In particular, the use of multicolor QD probes in immunohistochemistry is considered one of the most important and clinically relevant applications. At present, however, clinical applications of QD-based immunohistochemistry have achieved only limited success. A major bottleneck is the lack of robust protocols to define the key parameters and steps. Here, we describe our recent experience, preliminary results and detailed protocols for QD-antibody conjugation, tissue specimen preparation, multicolor QD staining, image processing and biomarker quantification. The results demonstrate that bioconjugated QDs can be used for multiplexed profiling of molecular biomarkers, and ultimately for correlation with disease progression and response to therapy. In general, QD bioconjugation is completed within 1 day, and multiplexed molecular profiling takes 1–3 days depending on the number of biomarkers and QD probes used.**

## INTRODUCTION

QDs are tiny light-emitting particles on the nanometer scale, and are emerging as a new class of fluorescent labels for biology and medicine<sup>1–11</sup>. In comparison with organic dyes and fluorescent proteins, QDs have unique optical and electronic properties such as size-tunable light emission, superior signal brightness, resistance to photobleaching and simultaneous excitation of multiple fluorescence colors. These properties are most promising for improving the sensitivity and multiplexing capabilities of molecular histopathology and disease diagnosis. Recent advances have led to highly bright and stable QD probes that are well suited for profiling genetic and protein biomarkers in intact cells and clinical tissue specimens<sup>12–14</sup>. In contrast to *in vivo* imaging applications where the potential toxicity of cadmium-containing QDs is a major concern, immunohistological staining is performed on *in vitro* or *ex vivo* clinical patient samples. As a result, the use of multicolor QD probes in immunohistochemistry (IHC) is likely one of the most important and clinically relevant applications in the near term.

In recent years, several groups have used QD probes for fluorescence immunostaining of fixed cells and tissue specimens<sup>15–21</sup>. However, medical applications of QD-based immunohistochemistry have not achieved widespread adaptation or significant clinical success. A major problem is the lack of robust protocols and experimental procedures to define the key factors and steps involved in QD immunohistochemical staining and data analysis. In particular, there are no consensus on methods for QD-antibody (QD-Ab) bioconjugation, tissue specimen preparation, multicolor QD staining, image processing and data quantification. Faced with these needs, we have developed antibody-conjugated QDs for multiplexed and quantitative (or semi-quantitative) IHC, and have achieved five-color molecular profiling on formalin-fixed and paraffin-embedded (FFPE) clinical tissue

specimens. We have also optimized the experimental procedures for QD bioconjugation, tissue specimen preparation, multicolor staining, image processing and analysis, and biomarker quantification<sup>6,12–14</sup>.

In this paper, we describe our recent experience, preliminary results and detailed experimental procedures. We also discuss the development of QD-Ab conjugates for quantitative and multiplexed IHC, an important but challenging goal that has not been achieved for diagnostic pathology. In contrast to standard hematoxylin and eosin tissue staining, multicolor QD staining allows the use of one antibody-QD conjugate to target a house-keeping gene product, thus providing an internal standard for signal calibration and quantification. This “ratiometric” staining approach to IHC can overcome many problems encountered with traditional methods<sup>22</sup>. In addition to clinical pathology, we envision that sensitive QD-based immunoassays represent a new direction for multiplexed detection of category A bioterrorism agents such as anthrax, plague, botulism and viral hemorrhagic fevers<sup>23</sup>.

## The procedure

A flowchart of the procedure with timing information is shown in **Figure 1**. Detailed protocols for QD-Ab conjugation (part 1) and for QD staining of cellular or tissue specimens (part 2) are given in the PROCEDURE section, followed by a discussion of imaging data acquisition, processing and analysis (part 3). A software tool for quantitative IHC (called Q-IHC) is given in **Box 1** and **Figure 2**. In addition, excellent protocols have been published for QD conjugation to luciferase (self-illuminating QDs)<sup>24</sup>, QD-protein conjugation via dihydrolipoic acid and non-covalent self-assembly<sup>25</sup>, and using bioconjugated QDs for tracking the motion of membrane molecules<sup>26</sup>.



### QD bioconjugation

As schematically illustrated in **Figure 3**, QD conjugation to biomolecules can be carried out by electrostatic binding, noncovalent biotin–avidin binding, direct covalent crosslinking and nickel-based histidine tagging. Mattoussi and co-workers<sup>25,27</sup> were the first to use an adaptor or fusion protein for IgG antibody coupling based on electrostatic interactions. The adaptor protein has a positively charged leucine zipper domain for electrostatic binding to QDs and a protein G domain for binding to the antibody Fc region. Using such a “bifunctional” adaptor, the Fc end of the antibody is connected to the QD surface, with the target-specific F(ab')<sub>2</sub> domains facing outward. For histidine-tagged peptides or antibodies, it is also possible to use the nickelnitrilotriacetic acid complex (Ni-NTA) as a bifunctional adaptor for QD bioconjugation. In this case, the nitriloacetic acid group is covalently linked to the QD encapsulation polymer whereas histidine-tagged antibodies bind to nickel ions (Ni<sup>2+</sup>) by chelation. In comparison with biotin–avidin binding, this “his-tag” method has several advantages such as a controlled orientation of the binding ligand (a histidine tag can be conveniently fused to proteins and peptides at a particular site), compact overall probe sizes and low production costs. Although the stability of the histidine–nickel attachment could be a problem under the harsh conditions of immunohistochemical staining, previous research has shown that the interaction of 6× His with Ni-NTA is virtually unaffected by high salt (up to 1 M), nonionic detergents (Triton X-100 or Tween 20 up to 1%, w/w), organic solvents, ethanol or glycerol to 30%, reducing agents (β-mercaptoethanol up to 10 mM) (see ref. 28) or highly denaturing conditions such as 8 M urea or 6 M guanidine hydrochloride<sup>29</sup>. Based on the 6-histidine epitope, we have not encountered major stability problems for the bioconjugated QDs in PBS buffer at room temperature (RT) for a period of 2–3 weeks at 4 °C.

Covalent QD conjugation is most commonly based on crosslinking reactions between amine and carboxylic acid groups (catalyzed by carbodiimide) (Step 1C), between amine and sulfhydryl groups (catalyzed by maleimide) (Step 1A) or between aldehyde and hydrazide functions. An advantage of the amine–carboxylic acid crosslinking method is that most proteins contain primary amine and carboxylic acid groups, and do not need chemical modifications before QD conjugation. In contrast, free and accessible sulfhydryl groups are rare in native biomolecules and are often unstable in the presence of oxygen. Another method for covalent conjugation involves oxidizing carbohydrate groups on the antibody's Fc portion to reactive aldehyde groups, which are then covalently linked to QDs (Step 1B). Because the carbohydrate's position is known on the antibody, this approach allows site-specific QD conjugation at relatively simple QD–Ab ratios. The properties and performance of these various QD–Ab conjugates are summarized in **Table 1**. In this contribution, we present four different, detailed methods for preparing QD–Ab conjugates for cell and tissue staining.

### Preparation of cell and tissue specimens

To optimize the procedures for specimen preparation, we have studied and compared fresh cells, frozen cells (stored at –80 °C), fixed cell pellets, as well as archived patient specimens (FFPE samples). Cells collected fresh from subculture are relatively easy to be stained and often show the best morphologies. For optimal

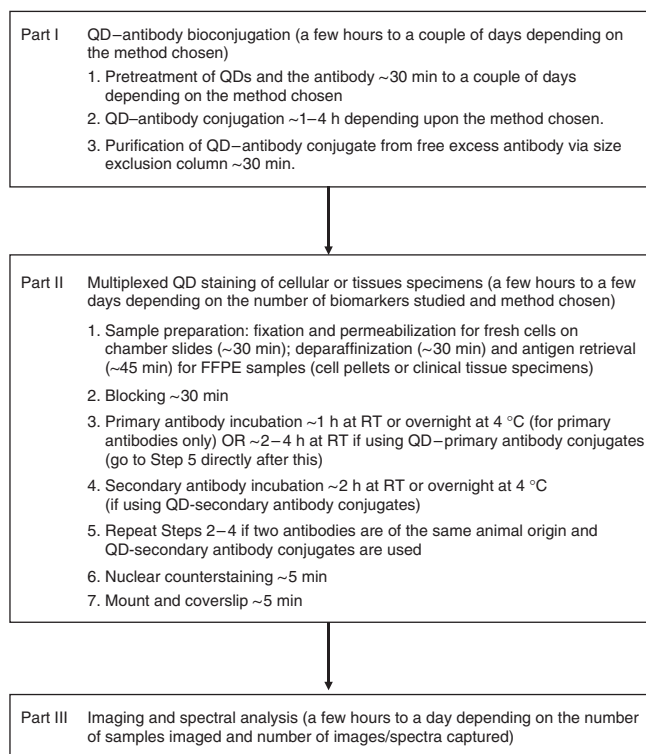


**Figure 1** | Flowchart and timing for QD conjugation and immunohistochemical staining of cells and tissue specimens.

cell membrane and cytoplasmic staining, however, the fresh cells often need to be fixed and permeabilized. Nuclear staining requires an additional proteinase K treatment step. For frozen cell specimens that are fixed with acetone/methanol before cryo-storage, no permeabilization is needed. For paraffin-embedded tissue specimens, we recommend an antigen retrieval step, as is commonly used in IHC<sup>30</sup>. This step is not always necessary, but antigen retrieval permits stronger staining signals. Typical antigen retrieval methods include heating, protease digestion and treatment under strong acidic conditions<sup>30</sup>. Selection of an antigen retrieval method depends much on the specific primary antibody to be used. We recommend the use of a pressurized cooker for heating (5 min at 120 °C) in citrate (pH 6.0) or EDTA (pH 8.0) buffer. Heating in EDTA buffer often leads to brighter staining signals, and is more suitable for low-abundance antigens or antigens with inaccessible epitopes. However, the pH of the buffers and the heating conditions could be too harsh for some tissue slides and could cause tissues to peel off. For best results, paraffin-mounted tissue specimens should be placed on coated slides (superfrost, positively charged) and baked to adhere firmly to the specimens, before subjecting to further steps of the described protocols. We present detailed procedures for QD staining of three types of samples: cells fresh from subculture (Step 2A), frozen cells samples (Step 2B) and FFPE cell/tissue specimens (Step 2C). Each sample type requires a different pretreatment method before QD staining.

### Multicolor QD staining

Depending on the types of QD bioconjugates and the primary antibodies used, multiplexed labeling of cells/tissue specimens can

## BOX 1 | Q-IHC - A SOFTWARE TOOL FOR QUANTITATIVE ANALYSIS OF IMMUNOHISTOCHEMICAL DATA

We have developed an integrated image processing and bioinformatics software tool (called Q-IHC) for quantitative analysis of biomarker expression and distribution in immunohistochemical (IHC) images (see **Figure 2**). In comparison to previous image processing software for automated feature extraction and quantitative analysis<sup>50,51</sup>, our software system is capable of handling imaging data from both traditional and QD-based IHC. To measure the distribution of labeled antigens, multiple slides of IHC imaging data are acquired to capture selected tissue structures. After image acquisition, an image processing module carries out automatic boundary identification, semi-automatic image segmentation, and color-based tissue classification based on biomarker staining. Then, an image analysis module quantifies the various biomarker features into numerical values. These values become distinct features and are used for comparison with clinical diagnosis. After validation by a physician, the quantitative data and rules describing biomarker features are stored in a database. This semi-automatic image processing and quantification system is designed to provide molecular profiling data that are more objective, more consistent, and more reproducible than completely manual or automated quantification methods. Our software tools process image files from slide scanners in Matlab, which is a collection of various engineering processing tools. We have designed a user-friendly graphical user interface that allows users to give input and feedback to improve the system quality.

The Q-IHC tool is available to academic and nonprofit research institutions from the Emory-Georgia Tech Center of Cancer Nanotechnology Excellence, funded by the National Cancer Institute (NCI), the Georgia Cancer Coalition (GCC), the Georgia Research Alliance (GRA), Emory University, and Georgia Institute of Technology. For further information on software download and deployment, go to: <http://www.bio-mi-lab.org>. Correspondence and requests concerning image analysis and biocomputing should be addressed to Dr. May D. Wang, Department of Biomedical Engineering, Georgia Tech and Emory University, 313 Ferst Drive, UA Whitaker Building 4106, Atlanta, Georgia 30332, USA, email address: [maywang@bme.gatech.edu](mailto:maywang@bme.gatech.edu).

be achieved by either direct or indirect staining procedures. For direct staining, each primary antibody is conjugated to a QD of a different color, and a mixture of several different QD–Ab conjugates is applied to the tissue specimen in a single step (Step 3B). Although this method is fast and efficient, some primary antibodies may not survive the QD conjugation process and their binding properties are likely altered by covalent modifications at either  $-NH_2$  or  $-COOH$  sites. Also, QD conjugation to primary antibodies does not work well when the original antibody buffer contains bovine serum albumin (BSA) or other culture medium proteins. Further, the reagents costs could become considerably high because each primary antibody is conjugated to just one type of QD, and none of the QD bioconjugates could

be used as a common reagent for staining of antigen or antibody classes.

These problems can be addressed by indirect QD staining, in which QD–secondary antibody conjugates are used to recognize primary antibodies (unlabeled) (Step 3A). The main advantages of this method are its flexibility, lower costs and the reduced constraint on primary antibodies. A typical multicolor labeling procedure would involve the following steps: blocking → 1st set of primary antibodies (each raised from a different animal species) → 1st QD–secondary antibody conjugates (each against a different animal species) → blocking → 2nd set of primary antibodies → 2nd set of secondary antibodies → so on. Despite these multiple blocking/staining/washing steps, we have achieved excellent results for five-color molecular profiling of cancer cells and tissue specimens (see below). It should be emphasized that careful control studies must be planned and included for data validation and interpretation. For QD–primary antibody conjugates, a negative control experiment is to saturate the antigens with isotype- and species-matched immunoglobulin molecules before QD staining. Additional controls should include the use of free QDs or BSA-QD conjugates to evaluate nonspecific binding and staining. For QD–secondary antibody conjugates, one key control is to determine the level of nonspecific binding when the primary antibody is purposely omitted from the staining protocols. For multiplexing purposes (Step 3C), QD–primary antibody conjugates will be the best choice. However, some antibodies may not be suitable for chemical modification. In these cases, QD–secondary antibody conjugates can be used instead. In the following, we present detailed procedures for both types of conjugates.

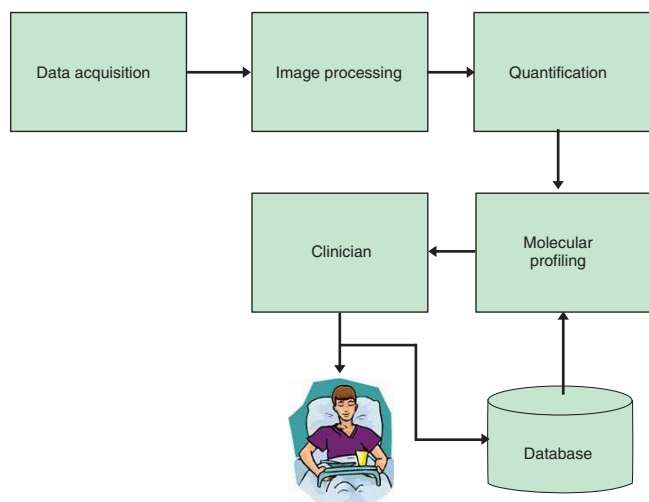


**Figure 2** | Block diagram of Q-IHC, an integrated software system for image processing and biomarker quantification of immunohistochemical data.

### Imaging data acquisition, processing, and analysis

In our laboratory, true-color fluorescence images are obtained by using an Olympus IX70 epifluorescence microscope equipped with

a long-pass filter, a mercury lamp, and a digital color CCD camera. Fluorescence spectroscopy is carried out by attaching a spectrometer to the microscope side port. By using objectives with different magnifications (zooming in and out), this micro-spectroscopic system allows one to acquire wavelength-resolved spectra from an individual cell as well as from a cluster of cells. At high magnifications (e.g., 100×), the spectra provide information on individual cells, while at low magnifications (2×, 10×), the spectra provide averaged signals for 10–100 cells. For data calibration, we calculate the average signal intensities (e.g.,  $40 \times 10^3$  arbitrary fluorescence units) for cell lines with over-expressed antigens (e.g., breast cancer cells with over-expressed Her2). Then we set this value as 100% and calculate the signal intensities of other cell lines as a percentage from this maximum. For clinical tissue specimens, we similarly measure the fluorescence intensity from a series of samples with the highest Her2 expression. This intensity is set as 100% and is used for further calculations. To ensure statistical validity, multiple spectra (30–50) of representative regions are taken and are averaged in the analysis.

**Image segmentation.** For segmentation of cell and tissue images, we have developed level-set algorithms using partial differential equations (PDEs) for identification of cellular regions versus non-cellular regions. The algorithms are independent of the initial conditions, and can automatically select the cell-region boundaries. For identification of special tissue structures, such as a prostate gland, we have developed a semi-automatic method that provides more user control for monitoring segmentation accuracy and sensitivity. Specifically, we developed a custom Graphics User Interface (GUI) based on the intelligent scissor (IS) algorithm<sup>31,32</sup>. This graphics interface allows the user to control the quantification process because the user often has *a priori* knowledge of staining color and biomarker locations (i.e., cell nucleus, cell membrane, cytoplasm, or the extracellular matrix). The user can start the segmentation process by moving the mouse cursor to a “region of interest” (ROI) such as an isolated cancer cell or a prostate gland, and then mark this region with a few “seed” points (user-selected points to delineate cell or gland boundaries). Then, the image processing system interactively computes multiple paths from the user-selected points to other neighboring points in the image, and extracts features such as edges (discontinuity in color or intensity) or areas (regions sharing similar textures). The one path that provides the optimal feature extraction is the solution. As one

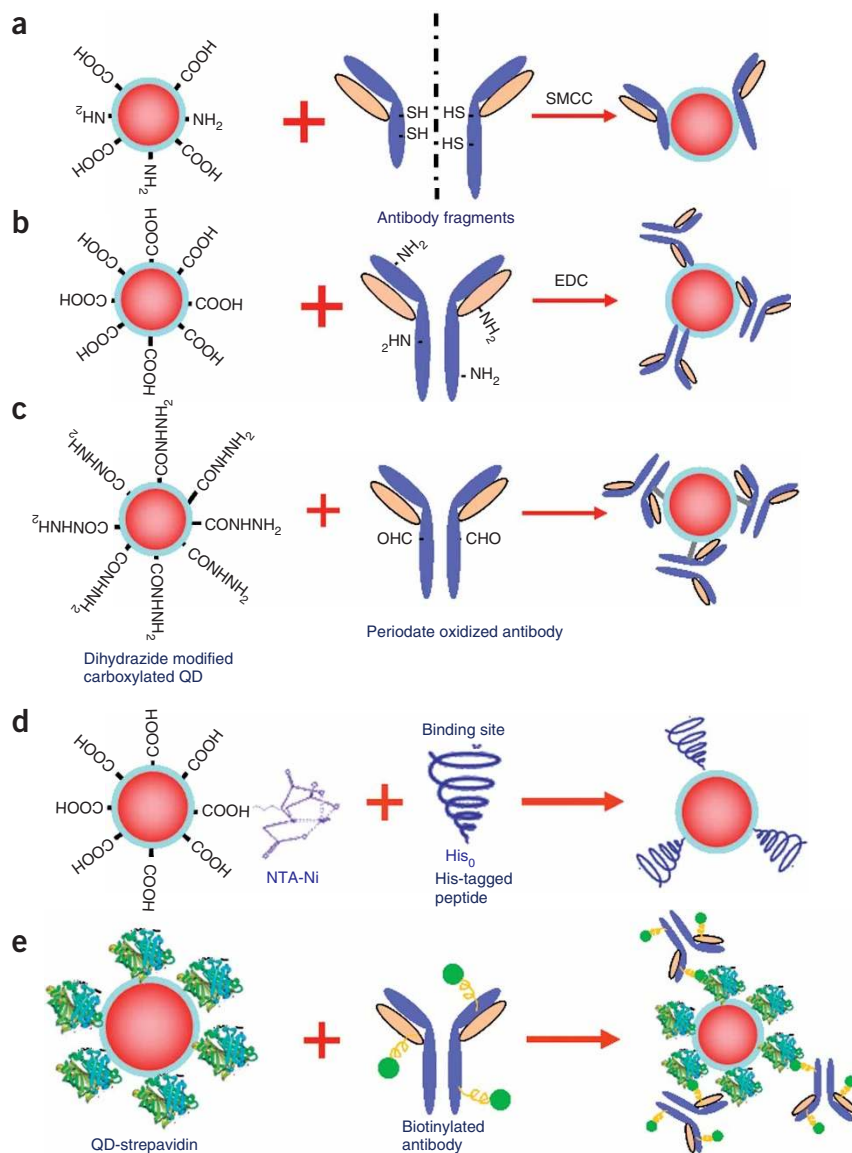


**Figure 3** | Schematic diagrams showing various methods for QD-antibody (QD-Ab) bioconjugation. (a) QD conjugation to antibody fragments via disulphide reduction and sulfhydryl-amine coupling; (b) covalent coupling between carboxylic acid (-COOH) coated QDs and primary amines (-NH<sub>2</sub>) on intact antibodies using EDC as a catalyst; (c) site-directed conjugation via oxidized carbohydrate groups on the antibody Fc portion and covalent reactions with hydrazide-modified QDs; (d) conjugation of histidine-tagged peptides or antibodies to Ni-NTA modified QDs; and (e) noncovalent conjugation of streptavidin-coated QDs to biotinylated antibodies.

example, **Figure 4** shows traditional IHC images of prostate tissue specimens in which features are extracted from the edges separating the pocket-shaped gland structure from other areas. The user can pick a starting “seed” by moving the mouse cursor to the top of one gland. As the mouse is placed by the user along one side of the gland, the image processing system will compute the connection from the “seed” point to all neighboring points. Multiple connecting paths will be generated, with the optimal path being labeled or highlighted in green color. This calculation occurs interactively in real time.

High computing efficiencies are achieved by using the optimal spanning tree based on Dijkstra’s graph searching algorithm<sup>33</sup>. This

**TABLE 1** | Methods for QD bioconjugation, conjugate characteristics and comparative performance for immunohistochemical staining.

Conjugation method	Sulfhydryl (covalent)	Amide (covalent)	Fc-sugar (covalent)	His-tag (noncovalent)	Biotin-avidin (noncovalent)
Conjugated ligand	Ab fragments	Whole Ab	Whole Ab	ScFv or Peptide	Whole Ab
Site specificity	Yes	No	Yes	Yes	No
Ligand orientation	Fixed	Random	Fixed	Fixed	Random or fixed <sup>a</sup>
Ab/QD ratio <sup>b</sup>	~ 4	~ 15	~ 15	~ 3–25	< 3
Staining specificity	Medium	Low	Medium	High	High
Staining brightness	Low	High	Very high	High	Medium
Background noise	Low	Medium	Low	Low	Low
Special conditions	Protein-free buffer	None	Carbohydrate	None	None
Reagent costs	Medium	Low	Medium	High	High
Overall performance	Fair	Poor	Excellent	Excellent	Good

Notes: the data were derived from the authors' laboratories at Emory University School of Medicine and Georgia Institute of Technology. Probe comparisons were made under identical experimental conditions. Performance evaluations were based on a number of parameters such as level of nonspecific staining, background noise and specific signal brightness. All QD-Ab conjugates are stable for 2–4 weeks at 4 °C.

<sup>a</sup>The orientation can be random or fixed based on the biotinylation method. <sup>b</sup>These are approximate estimates based on the number of functional groups on the QD and the molar ratio of starting materials under the assumption that 50% of the starting antibody molecules are conjugated to QDs. The actual number of antibodies per QD could vary depending on the reaction conditions.

search algorithm treats the image as a weighted graph. Each pixel represents a node with directed and weighted edges that connect with its eight adjacent neighbors. As the mouse cursor moves, the optimal path from the pointer position to the seed point is displayed. This path allows the user to select an optimal contour segment that visually corresponds to a portion of the desired object boundary. As the mouse cursor moves, the optimal path from the

pointer position to the “seed” point is calculated. When the mouse pointer comes in proximity to an object edge, a live wire boundary snaps to and wraps around the object of interest<sup>31,32</sup>, as highlighted in red contour color in **Figure 4**. If the user finds the contour segment visually corresponds to a portion of the desired object boundary, double clicking the mouse fixes the contour and changes its color to green. This design enables the user to play a part in the process of computer-based contour feature extraction, leading to more reliable and more repeatable results. After the cellular and tissue shapes are identified by image segmentation, further data analysis will only focus on ROIs. The key next step is to classify each pixel to a biomarker or to the background by using K-means clustering<sup>34</sup>.

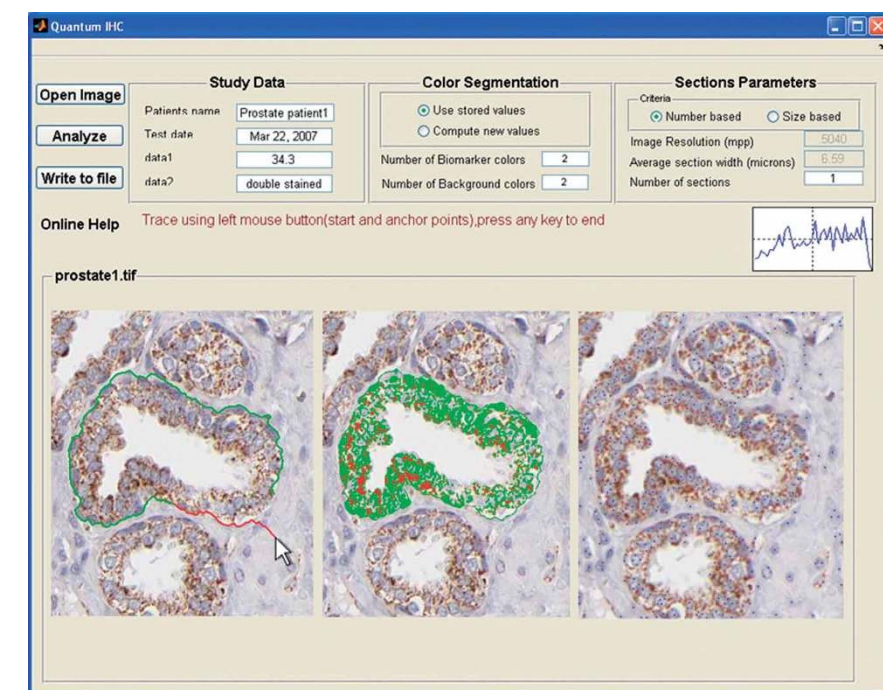


**Figure 4** | Computer screen showing prostate tissue specimens stained with traditional IHC and the graphical interface for image analysis and biomarker quantification. Left panel: the user can pick a starting “seed” by moving the mouse to the top of one prostate gland. As the mouse is placed by the user along one side of the gland, the image processing system will compute the connection from this “seed” point to all neighboring points. Multiple possible connecting paths will be generated, and then the optimal path will be labeled (i.e., highlighted in green color edge). This calculation occurs interactively in real time. Middle panel: the use of K-means clustering to segment QD-stained tissue images, with cellular structures being highlighted by light green and light red colors. Right panel: automated counting of brown staining cells (red dots) and blue-staining cells (blue dots). The IHC images openly available from the Human Proteome Organization (HUPO) are used in this analysis, demonstrating the broad utility of our software system. Detailed staining information: antibody CAB002311, protein EnsEMBL ID: ENSP00000304146, netrin receptor DCC precursor in prostate tissue; see <http://www.proteinatlas.org>.

**K-means clustering.** In addition to determining the staining intensity of biomarkers, it is important to know the location of biomarkers in an ROI, especially for multiplex-QD labeled cell and tissue specimens. We have used the K-means algorithm because it has three distinctive advantages: (a) no requirement for human interaction, (b) ease of implementation, and (c) high performance. K-means is a widely used technique for clustering of multi-spectral data<sup>34</sup>, and is based on the sum of least squares criterion. For example, in two-color QD staining of prostate cancer tissues, we can define each color of the biomarker and the background as one cluster. For k-1 biomarker and the background, the first step is to define k centroids (center positions), one for each cluster. These centroids may be initialized by predefined values, or may be placed far away from each other to avoid local minima convergence. The next step is to take each point belonging to a given data set and associate it to the nearest centroid. When this initial grouping is



done, we need to recalculate  $k$  new centroids of the clusters resulting from the previous step. After we have these  $k$  new centroids, a new binding is established between the same data set points and the nearest new centroids. During this iterative process, the  $k$  centroids keep changing their locations step by step until they are stabilized (that is, the  $k$  centroid positions no longer move or change). During this iterative process, the algorithm aims to minimize an objective function, in this case a squared error function:

$$J = \sum_{j=1}^k \sum_{i=1}^n \left\| x_i^{(j)} - c_j \right\|^2$$

where  $\left\| x_i^{(j)} - c_j \right\|^2$  is a chosen distance between a data point  $x_i^{(j)}$  and the cluster center  $c_j$ , and is an indicator of the distance of  $n$  data points from their respective cluster centers. This K-means color segmentation can be used for both traditional IHC (Figure 4) and QD-IHC (Figure 5) to quantify biomarkers and background, and also to count cells.

Figure 5 shows an example of using two-color QD probes to stain two biomarkers (p53 and EGR-1) in prostate cancer tissues, together with the detection of blue fluorescence as the tissue background. The ROIs are identified by using 3-means ( $k = 3$ ), and are highlighted in red (p53), green (EGR-1), and blue (background). The three clusters are combined together to show the distribution of each biomarker and the background.

A potential problem of the K-means algorithm is that it may converge to a local minimum instead of the optimal global solution. Thus, additional features are added to make the algorithm robust and adaptable to significant variations in staining densities and lighting conditions: (i) to allow the user (if required) to initialize the clustering algorithm by manually marking starting seed points; and (ii) to allow the user to select the specific type of staining and the number of biomarkers. As a result, our K-means algorithm is able to process traditional IHC as well as multiplexed QD stained slides on the same platform. It can also detect different types of staining color themes (e.g., brown-colored staining in standard IHC and orange-colored fluorescence in QD staining).

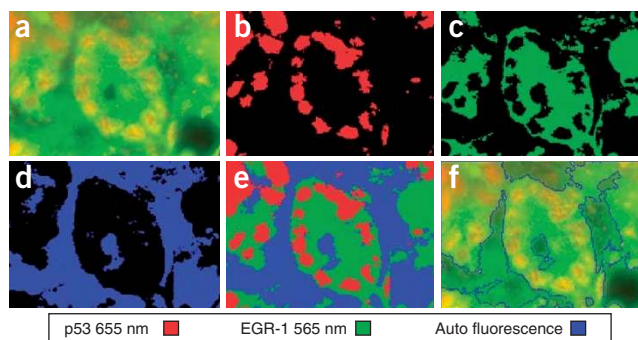


**Figure 5** | Multiplexed QD IHC images of clinical FFPE (formalin fixed, paraffin embedded) prostate tissue specimens, and quantitative analysis of cancer biomarkers and tissue background fluorescence. The fluorescence images were obtained with UV excitation, with the p53 marker stained red with QD655, the EGR-1 marker stained green with QD565, and the tissue background observed as blue. The color maps show the location where a biomarker (or the tissue background) is more pronounced than others. (a) Original multicolor image; (b) p53 protein (red); (c) EGR-1 protein (green); (d) tissue background fluorescence (blue); (e) combined map of dominant markers and background; and (f) automated boundary segmentation using level-set algorithms.

**Data quantification.** Because the amount of biomarker in the tissue is proportional to the amount of staining, and because the fluorescence intensity (or optical density) is proportional to the amount of staining, it is possible to quantify biomarker expressions by fluorescence intensity or optical density measurements. For this purpose, the biomarkers detected during the image processing are converted into numeric values. Key parameters are extracted such as biomarker staining intensities, background intensities, and the relationship of biomarker to background areas (this relative value is used to alleviate potential biases introduced by absolute numbers). These parameters pertaining to the complete ROI as well as each subsection are stored in a database. Analysis and classification of these parameters can provide information on the molecular anatomy of normal and diseased cells. For clinical outcome studies, the biomarker expression profiles are correlated with datasets that are already validated and stored in a database.

## MATERIALS

### REAGENTS

- Antibodies: E-cadherin (Santa Cruz Biotechnology, cat. no. sc7870), N-cadherin (Abcam, cat. no. ab12221), vimentin (Santa Cruz Biotechnology, cat. no. sc6360), EF1alpha (Upstate, cat. no. 05-235) and RANKL (Santa Cruz Biotechnology, cat. no. sc-52951)
- Custom-made CdSe/ZnSe/ZnS QDs with fluorescence emission peaks at 530 and 650 nm (provided by Andrew Smith of Georgia Tech and Emory University)
- QD655 primary antibody conjugation kit (Invitrogen, cat. no. Q2202MP)
- QD655 nanocrystals (amino, 4  $\mu$ M) (included in the primary antibody conjugation kit; Invitrogen, cat. no. Q2202MP) SMCC (4-(maleimido-methyl)-1-cyclohexanecarboxylic acid N-hydroxysuccinimide ester; included in the primary antibody conjugation kit; Invitrogen, cat. no. Q2202MP) QD nanocrystals (carboxylated, 8  $\mu$ M) (Invitrogen, cat. no. Q21321MP)
- Dithiothreitol (DTT) (included in the primary antibody conjugation kit; Invitrogen, cat. no. Q2202MP)
- Adipic acid dihydrazide (ADH) (Sigma, cat. no. A0638)
- EDC ((N-(3-dimethylaminopropyl)-N'-ethylcarbodiimide hydrochloride; Fluka, cat. no. 03450)

- Dialysis tubing (MWCO: 50 kDa, Spectral Laboratories, cat. no. 132128)
- Sodium periodate (Pierce, cat. no. 20504)
- PBS buffer (10 $\times$ , pH 7.2) (VWR, cat. no. EM6507)
- NHS (N-hydroxysuccinimide; Pierce, cat. no. 24500)
- Methanol (Sigma, cat. no. 179337)
- QD-streptavidin nanocrystals (1  $\mu$ M) (Invitrogen, cat. no. Q10121MP)
- Biotin-LC-hydrazide for size-directed biotinylation (Pierce, cat. no. 21340)
- NHS-PEO-biotin for random biotinylation (Pierce, cat. no. 21330)
- Triblock copolymer consisting of a poly-butylacrylate segment, a poly-ethylacrylate segment and a poly-methacrylic acid segment (see details below) (Sigma, MW = 100 kDa)
- Deionized (DI) water (18 M $\Omega$ ) (Millipore Milli-Q, CDOF01205)
- Normal goat serum (Vector Laboratories, cat. no. S-1000)
- BSA (Sigma, cat. no. A2153)
- DAPI nuclear stain (Sigma, cat. no. D9564)
- Mounting media (Biomedica, gel-mount, cat. no. M-01)

### EQUIPMENT

- NAP-5 columns (GE Healthcare, cat. no. 17-0853-01)
- Gel filtration columns (Pierce, cat. no. 29920)
- Superdex 200 media (GE Healthcare, cat. no.17-1043-10)

- Syringe and plastic tubing (included in the Invitrogen primary antibody conjugation kit)
- Stand and racks to hold the columns upright (Fisher, cat. no. 14-809-136 and 03-448-17)
- Centrifuge tubes (1.5 ml; VWR, cat. no. 87003-290)
- Non-stick centrifuge tips (1.5 ml; VWR, cat. no. 20170-650)
- Hydrophobic pen **▲ CRITICAL** Not all hydrophobic pens used in IHC would work for QD staining; some of them may contain organic solvents that may “quench” QDs. According to our experience, try to stick with the ImmunoEdge pen from Vector Laboratories.
- Concentrator (MWCO: 50 kDa) (Millipore, cat. no. 42415)
- Pipettors (Corning Lambda, cat. nos. CRSC001, CRSC003, CRSC005 and CRSC006)
- Pipette tips (Fisher Scientific, cat. no. 02-707-136; VWR, cat. nos. 53508-810 and 83007-376)
- Transfer pipette (Fisher Scientific, cat. no. 13-711-7)
- Staining jar (VWR, cat. no. 25460-00)
- Lab-tek chamber slide system (sterile) (VWR, cat. no. 62407-296)
- Coverslips (VWR, cat. no. 48404-454)
- 3-D rotator (Lab-line, cat. no. 4630)
- UV/Vis spectrometer (Shimadzu UV-2401 PC)
- Fluorescence spectrometer (Roper Scientific, model SpectraPro 150)
- UV lamp (VWR, UVP/UVL-56)
- Centrifuge machine (VWR, C0175-VWR)
- Pressure cooker and steamer (DAKO, model S2800)
- Epifluorescence microscope (Olympus, model IX70)
- Spectral imaging microscope (CRI Inc., Nuance System with liquid crystal tunable filter tuning between 400 and 720 nm)
- Rotating evaporator (Rotavapor R-3000; Buchi Analytical Inc.)

#### REAGENT SETUP

**Amphiphilic block copolymers** A triblock copolymer (consisting of a poly-butylacrylate segment, a poly-ethylacrylate segment and a poly-methacrylic acid segment with a molecular mass of approximately 100,000 Da) was chemically modified for surface encapsulation of custom-made and Crystalplex TriLite (ternary alloyed semiconductor) QDs<sup>6</sup>. For this purpose, the original polymer [poly(*tert*-butyl acrylate-*co*-ethyl acrylate-*co*-methacrylic acid), cat. no. 444790, Sigma-Aldrich] dissolved in dimethylformamide is reacted with *n*-octylamine at a polymer/octylamine molar ratio of 1:40, using ethyl-3-dimethyl amino propylcarbodiimide (EDAC, threefold excess of *n*-octylamine) as a crosslinking reagent (reaction conditions: overnight, RT and normal atmosphere). The product yields are generally greater than 90% owing to the high EDAC coupling efficiency in dimethylformamide (determined by a change of the free octylamine band in thin-layer chromatography (use 1:1 mixed CHCl<sub>3</sub>:MeOH as the mobile phase, and stain for unreacted amines using ninhydrin stain (300 mg ninhydrin dissolved in 100 ml *n*-butanol and 3 ml acetic acid)). The reaction mixture is dried with a rotavap (Rotavapor R-3000, Buchi Analytical Inc.). The resulting oily liquid is precipitated with water and is rinsed with water five times to remove excess EDAC and other by-products. After vacuum drying, the

octylamine-grafted polymer is resuspended in an ethanol/chloroform mixture and stored for use.

**QD encapsulation and solubilization** Using a 3:1 (v/v) chloroform/ethanol solvent mixture, TOPO-capped QDs are encapsulated by the amphiphilic triblock polymer. A polymer-to-QD ratio of 5:10 is used because molecular geometry calculations indicate that at least four polymer molecules would be required to completely encapsulate one QD. Indeed, stable encapsulation (e.g., no aggregation) is not achieved at polymer/dot ratios less than 4:1. After vacuum drying, the encapsulated dots are suspended in a polar solvent (aqueous buffer or ethanol) and purified by gel filtration.

**QD activation with EDC/NHS in methanol** To 15  $\mu$ l QDs (8  $\mu$ M), add 3  $\mu$ l EDC (2.2 mM in methanol) and 3  $\mu$ l NHS (4 mM in methanol), followed by another 9  $\mu$ l methanol, yielding a total volume of 30  $\mu$ l. Leave this at RT for 30 min.

**Antibody biotinylation** Site-directed biotinylation is performed using biotin-hydrazide and periodate-oxidized antibodies (detailed procedures are given below) and random biotinylation is performed using NHS-PEO-biotin through amine groups on the antibody (refer to Pierce website for detailed procedures).

**Antibody oxidation with sodium periodate** (a) Dissolve antibody in 0.01 M sodium phosphate, 0.15 M NaCl, pH 7.2 (final concentration: 10 mg ml<sup>-1</sup>). (b) Dissolve sodium periodate in water (final: 0.1 M), protect from light; immediately add 100  $\mu$ l of sodium periodate to 1 ml of the antibody solution (1.5 mg ml<sup>-1</sup>); mix to dissolve, protect from light. (c) React in the dark for 30 min at RT. (d) Purify by dialysis overnight against PBS (dialysis tubing, MWCO: 50 kDa).

**Antibody sample for Step 1A** Before an antibody of interest is reduced, it should be purified and formulated in PBS at a concentration of 1 mg ml<sup>-1</sup>. The antibody solution must be free of blood/serum, ascites and other proteins such as BSA.

#### EQUIPMENT SETUP

**Spectral imaging** Wavelength-resolved spectral imaging is carried out by using a spectral imaging system (CRI Inc.), which consists of a optical head that includes a liquid crystal tunable filter (LCTF, with a bandwidth of 20 nm and a scanning wavelength range of 400–720 nm), an optical coupler and a cooled, scientific-grade monochrome CCD camera, along with image acquisition and analysis software. The tunable filter can be automatically stepped in 10-nm increments from 580 to 700 nm while the camera captures images at each wavelength with constant exposure. Overall acquisition time is about 10 s. The 13 resulting TIFF images are loaded into a single data structure in memory, forming a spectral stack with a spectrum at every pixel. With spectral imaging software, small but meaningful spectral differences can be rapidly detected and analyzed.

**Quantitative imaging and spectroscopy** An inverted Olympus microscope (IX-70) with a broadband light source (ultraviolet 330–385 nm and blue 460–500 nm) and long-pass interference filters (DM 400 and 510, Chroma Tech), plus a digital color camera (Nikon D1) and a single-stage spectrometer (SpectraPro 150, Roper Scientific) are used for quantitative imaging and spectroscopy.

## PROCEDURE

### Conjugation

**1|** Conjugate antibody fragments to QDs using one of the four methods: conjugations using SMCC (option A), conjugation of antibodies to QD nanocrystals via oxidized Fc-carbohydrate groups (option B), direct conjugation of antibodies to QD nanocrystals through amine-carboxylic acid coupling (option C) or indirect conjugation of biotinylated antibodies to streptavidin-coated QDs (option D). In option A, disulfide bonds in the hinge region that hold the two heavy chains together are selectively cleaved to create two antibody fragments, each containing free sulfhydryls and an antigen-binding site.

Many immunoglobulin molecules are glycoproteins that can be periodate-oxidized to reactive aldehyde residues (option B). Polyclonal IgG molecules contain carbohydrate in the Fc portion of the molecule. This is sufficiently removed from the antigen-binding sites to allow conjugation to take place through the sugar chains without compromising binding specificity or affinity<sup>35</sup>. Periodate-oxidized antibodies can then be conjugated to hydrazide groups<sup>36</sup>. Carboxylated QDs can be modified with ADH to generate hydrazides on the QD surface<sup>36</sup>, which are then conjugated to oxidized antibodies through aldehyde-hydrazide covalent chemistry.

Antibody molecules possess a number of functional groups that are suitable for QD conjugation. Crosslinking reagents can be used to target lysine primary amine and N-terminal amine groups (option C). However, the distribution of these functional groups within the three-dimensional structure of an immunoglobulin molecule is nearly uniform throughout the surface

topology. For this reason, conjugation procedures using these groups often result in random orientation of the antibody in the QD bioconjugates, blocking some antigen-binding sites. In comparison with site-directed conjugation, the random coupling procedures do not place any special requirements on the antibody.

**■ PAUSE POINT** Once prepared, the QD–Ab conjugates can be stored for about 4–6 weeks. Beyond this storage period, staining still works but the quality is fairly poor. The problem is that most antibodies need to be stored at  $-20\text{ }^{\circ}\text{C}$  while QD samples at  $4\text{ }^{\circ}\text{C}$ . If the QD–Ab conjugates are stored at  $4\text{ }^{\circ}\text{C}$  for too long, the antibodies lose binding affinity and specificity.

**(A) Conjugation of primary antibody fragments to QDs ● TIMING 2–4 h**

- (i) Mix QD with SMCC for 1 h at RT. A 125  $\mu\text{l}$  portion of stock QD solution ( $4\text{ }\mu\text{M}$ ) is mixed with 13.8 mM SMCC, leading to a final concentration of 1 mM SMCC.
- (ii) Remove SMCC via size-exclusion column: remove both the caps of the NAP-5 column to allow as-supplied liquid to elute through; equilibrate gel with 10 ml exchange buffer; cap the bottom of the column while there is still liquid above the gel bed; add the reaction sample to the column; elute the exchange buffer and collect colored elute.
- (iii) Antibody reduction: antibody is reduced with DTT to expose free sulfhydryl groups. Add 6.1  $\mu\text{l}$  DTT to 300  $\mu\text{l}$  antibody ( $1\text{ mg ml}^{-1}$ ) and allow the reaction to proceed for 30 min at RT.
- (iv) Remove DTT via size-exclusion column: add 20  $\mu\text{l}$  of dye-labeled marker (included in the QD655 primary antibody conjugation kit (Invitrogen, cat. no. Q2202MP)) to the reduced solution; pass the solution through NAP-5 column; and collect colored elute.
- (v) Mix activated QD from Step 1A(ii) and reduced antibody from Step 1A(iv) and incubate the reaction for 1 h at RT ( $20\text{--}25\text{ }^{\circ}\text{C}$ ).
- (vi) Prepare 10 mM of  $\beta$ -mercaptoethanol stock immediately before use (working concentration should be  $100\text{ }\mu\text{M}$ , which corresponds to 10.1  $\mu\text{l}$  of 10 mM  $\beta$ -mercaptoethanol solution for a 1.0 ml reaction solution).
- (vii) Quench the reaction (Step 1A(v)) with  $\beta$ -mercaptoethanol for 30 min at RT.
- (viii) Concentrate down to 20  $\mu\text{l}$  or less with spin filters (MWCO 50 kDa).
- (ix) Separate the QD–Ab conjugates from free antibodies using gel filtration filled with Superdex 200 media. Collect only the first ten drops of the eluted solution once color appears (use UV lamp to help visualize the color) in the column's 'dead space'.
- (x) QD–Ab conjugates are now ready for cell/tissue staining purposes.

**? TROUBLESHOOTING**

**(B) Conjugation of antibodies to QD nanocrystals via oxidized Fc-carbohydrate groups ● TIMING 4–6 h, 2 days if dialysis is chosen for purification**

- (i) For 1 ml reaction solution, add 12.5  $\mu\text{l}$  QD nanocrystal stock (carboxylated,  $8\text{ }\mu\text{M}$ , and yielding a final concentration of 100 nM), 4  $\mu\text{l}$  of 5 mM EDC stock (final concentration is  $20\text{ }\mu\text{M}$ ) and 5.1  $\mu\text{l}$  ADH solution (dissolved in PBS,  $3.2\text{ }\mu\text{g }\mu\text{l}^{-1}$ ) (16.4  $\mu\text{g}$  total).
- (ii) Mix well and react for 4 h at RT.
- (iii) Remove excess ADH and EDC by dialysis overnight against 2 liters of PBS (dialysis tubing, MWCO: 50 kDa). (The selection of dialysis over size-exclusion column is a personal preference and is based on available supplies in the laboratory, not for a scientific reason. It is however important to minimize the loss of QDs and antibodies as both reagents are expensive.)
- (iv) Dissolve antibody in 0.01 M sodium phosphate, 0.15 M NaCl, pH 7.2 (final:  $10\text{ mg ml}^{-1}$ ).
- (v) Dissolve sodium periodate in water (final: 0.1 M) and protect from light by wrapping the reaction tube with aluminum foil or keep the tube in a dark room.
- (vi) Immediately add 100  $\mu\text{l}$  of sodium periodate to 1 ml of the antibody solution ( $1.5\text{ mg ml}^{-1}$ ); mix to dissolve, protect from light as above.
- (vii) React in the dark for 30 min at RT.
- (viii) Purify by dialysis overnight against PBS (dialysis tubing, MWCO: 50 kDa).
- (ix) Mix QD–hydrazide and periodate-oxidized antibody at a QD:antibody molar ratio of 1:30 and react for 2 h at RT.
- (x) Concentrate the reaction solution to 20  $\mu\text{l}$  or less for the next step.
- (xi) Separate the QD–Ab conjugates from free antibodies by gel filtration using Superdex 200 as the media. Collect the first ten drops of colored elute (if QD concentration is too low to be visible, use a UV lamp to illuminate).

**? TROUBLESHOOTING**

**(C) Direct conjugation of antibodies to QD nanocrystals through amine–carboxylic acid coupling ● TIMING ~ 6 h**

- (i) Mix activated QDs with antibody ( $1\text{ mg ml}^{-1}$  in PBS) and react for 4 h at RT; keep the amount of methanol below 4–5% of total reaction volume; QD:antibody molar ratio is  $\sim 1:30$ ; final concentration of QD in the reaction should be around 50 nM.
- (ii) Separate QD–Ab conjugates from excess free antibodies via gel filtration using Superdex 200 columns.
- (iii) Measure collected elutes via UV–visible absorption and fluorescence spectroscopy.

**? TROUBLESHOOTING**

**(D) Indirect conjugation of biotinylated antibodies to streptavidin-coated QDs ● TIMING 3–4 h**

- (i) Mix biotin-LC-hydrazide with oxidized antibody (biotin/antibody molar ratio is 4:1, and the final biotin-hydrazide concentration is 5 mM) and react at RT for 2 h.



## PROTOCOL

- (ii) Purify three times using spin filters (MWCO: 50 kDa) (spin at 5,000 r.p.m. and dilute 1:10 with PBS, each time).
- (iii) Mix biotinylated antibody with QD–streptavidin (volume ratio: 1:1) and react at RT for 1 h.
- (iv) Separate QD–Ab conjugates from free antibodies using gel filtration (Superdex 200). The resulting QD–Ab conjugates are now ready for staining purposes.

2| Prepare cells for staining by following the steps in options A–C for fresh cells from cultures, frozen cells and FFPE tissues, respectively.

### (A) Fresh cells from cultures ● TIMING 1–2 h

- (i) Culture cells in multiwell chamber slides overnight or 2 days till they reach about 50–80% confluency.
- (ii) Aspirate off media with transfer pipettes.  
**! CAUTION** Avoid using motorized pipettors as this will cause cell wash-off owing to the high shear stress.
- (iii) Wash with PBS briefly.
- (iv) Fix and permeabilize with 3.7% formaldehyde/0.1% Triton X-100/PBS for 20 min at RT.
- (v) Wash with PBS three times, each for 5 min.
- (vi) (Optional, for nuclear staining only) Incubate with proteinase K (30  $\mu\text{g ml}^{-1}$  in SDS) for 45 min to 1 h at 37 °C.  
**! CAUTION** We note that the use of proteinase K can cause problems because this enzyme nonspecifically cuts all proteins (including the antigens of interest). This problem can be alleviated by controlling the proteinase concentration and the time of incubation. For nuclear antigens, we have not experienced major problems. It is likely that proteinase K degrades intracellular matrix proteins and opens up the nuclear envelope, but does not cause significant damage to antigens in the nuclei if the incubation time is relatively short (45 min to 1 h). However, adequate controls for the presence of antigen epitopes (e.g., by extraction immunoblotting before and after proteinase K treatment) are still necessary. This is especially true for archival FFPE tissues, which may present a range of different fixation conditions and may be differentially susceptible to proteinase digestion.

### (B) Frozen cells ● TIMING 0.5–1 h

- (i) Remove cell chamber slides from –80 °C freezer (frozen cells can be prepared by fixing the cells in ice-cold acetone for 20 min at –20 °C before transferring to –80 °C freezer).
- (ii) Thaw (leave the cell chamber at RT and wait till it warms up).
- (iii) Wash with PBS 2–3 times.

### (C) FFPE tissues ● TIMING 1–2 h

- (i) Deparaffinize by immersing the slides in xylene for 5 min (repeat three times).
- (ii) Dehydrate in 100% ethanol for 2 min (repeat twice), 2 min in 95% ethanol (repeat twice) and 2 min in 75% ethanol (repeat twice).
- (iii) Rinse with DI water for 2 min.
- (iv) Perform an antigen retrieval step (by heat). Some antigens may require other methods such as proteinase K treatment. Pressure-cook (DAKO) or steam for 40 min; use citrate buffer (pH 6.0) for antigens with high abundance; use EDTA buffer (pH 8.0) for low-abundance antigens.  
**! CAUTION** When using EDTA buffer, make sure tissue sections are on superfrost or positively charged slides; otherwise, tissue will float off slide during antigen retrieval.
- (v) Cool for 20 min.
- (vi) Wash with PBS three times, 5 min each.

3| Stain the cells using antibody conjugates. The procedure will depend on whether you are using QD–secondary antibody conjugates (option A), QD–primary antibody conjugates (option B) or multiplexed QD staining on FFPE samples (option C).

### (A) Using QD–secondary antibody conjugates ● TIMING 4–6 h for one set of biomarkers (a “set” is defined as containing antibodies from different animal species)

- (i) Block with 2% BSA/5% goat (or rabbit) serum/PBS for 30 min at RT.  
**▲ CRITICAL STEP** Blocking serum needs to be of the same animal origin as the secondary IgG.
- (ii) Incubate the first set of primary antibodies (2–10  $\mu\text{g ml}^{-1}$  in blocking buffer) for 1 h at RT.
- (iii) Wash with PBS three times, 5 min each. Incubate the first set of QD–secondary antibodies (20 nM in 2% BSA/PBS solution) for 2 h at RT or overnight at 4 °C.
- (iv) Wash with PBS vigorously three times, 5 min each.
- (v) Repeat Steps (i)–(iii) for additional sets of biomarkers.
- (vi) Wash with PBS three times, 5 min each.
- (vii) Counterstain cell nuclei with DAPI (100 ng  $\text{ml}^{-1}$  in water) for 5 min, then wash with DI water for 5 min.

(viii) Mount and coverslip. Store in dark at 4 °C before microscopic viewing.

**! CAUTION** If cross-contamination is a problem during successive rounds of antibody staining, this problem can be alleviated by incubating the samples with unlabeled secondary IgGs to saturate the unbound binding sites before incubation with the subsequent set of primary antibodies.

**? TROUBLESHOOTING**

**(B) Using QD–primary antibody conjugates ● TIMING 3–5 h**

(i) Block with 10% horse serum for 30 min at RT.

(ii) Incubate with QD–primary antibody conjugates: (a) membrane antigen: 20–30 nM, 2 h at RT; (b) nuclear antigen: 40–60 nM, 4 h at RT. Pause for thoughts: one potential limitation is that the nuclear antigens might not be accessible to staining by large QD probes. In our hands, we did not see significant differences among 655, 605 and 565 nm QDs for nuclear staining. Theoretically, one would prefer smaller QDs for nuclear staining, but practically we have not found much difference. The reason is perhaps that our tissue specimens are cut and that the nuclear antigens are exposed for antibody binding. For deeper QD tissue penetration, we have used detergents to good effect.

(iii) Wash with PBS three times, 5 min each.

(iv) Nuclear counterstaining: (a) cell nuclei can be stained with DAPI (100 ng ml<sup>-1</sup> in water) for 5 min; (b) wash with DI water for 5 min.

(v) Mount and coverslip. Store in dark at 4 °C before microscopic viewing.

**? TROUBLESHOOTING**

**(C) Multiplexed QD staining on FFPE samples ● TIMING overnight**

(i) Draw a circle around the tissue section with a hydrophobic pen; this is to minimize the amount of reagents in the following steps.

(ii) Block with 2% BSA/5% goat serum/PBS for 30 min at RT.

(iii) Incubate primary antibodies for 1 h at RT or overnight at 4 °C, depending on the affinity of the antibody.

(iv) Wash with PBS three times, 5 min each.

(v) Incubate QD–secondary antibody conjugates overnight at 4 °C.

**▲ CRITICAL STEP** Overnight at 4 °C always works, 2 h at RT may also work for some antigens; but 1 h at RT is usually not sufficient. We note that the antibody quality (i.e., binding affinity and specificity) plays a major role in determining QD staining success or failure. For example, the antibodies from US Biological should be incubated for at least 30 min at RT for nuclear antigen staining even in traditional IHC. When conjugated to QDs, we see nuclear staining after 1 h at RT, but more “gentle” and complete antigen binding is achieved after overnight incubation at 4 °C.

(vi) Wash with PBS vigorously for three times, 5 min each.

(vii) Counterstain with DAPI (100 ng ml<sup>-1</sup>) for 5 min at RT.

(viii) Wash with DI water at RT for 5 min.

(ix) Mount with gel-mount (aqueous media) and coverslip.

(x) Place slides in the slide-holder and store at 4 °C.

**? TROUBLESHOOTING**

**? TROUBLESHOOTING**

**Step 1A**

Unsuccessful conjugation is often due to the presence of other disulfide-containing molecules in the antibody medium or buffer. QD conjugation should be confirmed by running agarose or PAGE gels showing size differences between conjugated and unconjugated antibodies and QDs.

**Step 1B**

Aggregate formation: EDC/ADH concentration too high; unsuccessful conjugation: antibody does not contain sugar group (e.g., some monoclonal antibodies). Successful conjugation should be confirmed by running agarose or PAGE gels showing size changes.

**Step 1C**

Aggregate formation: QD concentration too high or too much EDC. Successful conjugation should be confirmed by running agarose or PAGE gels.

**Steps 3A–C**

First, check the quality of QD–Ab conjugates by spreading a small drop on a coverslip and examining it under a fluorescence microscope. Some conjugates may contain aggregates owing to inappropriate handling or storage. It should be noted, however, that even new samples of QD–IgG conjugates from commercial sources could contain lots of aggregates. Check the slides under a microscope after each QD staining step; if there is too much staining, reduce the amount of primary antibody or QD–secondary antibody; if no staining or staining is too weak, increase the antibody concentrations or incubation time.



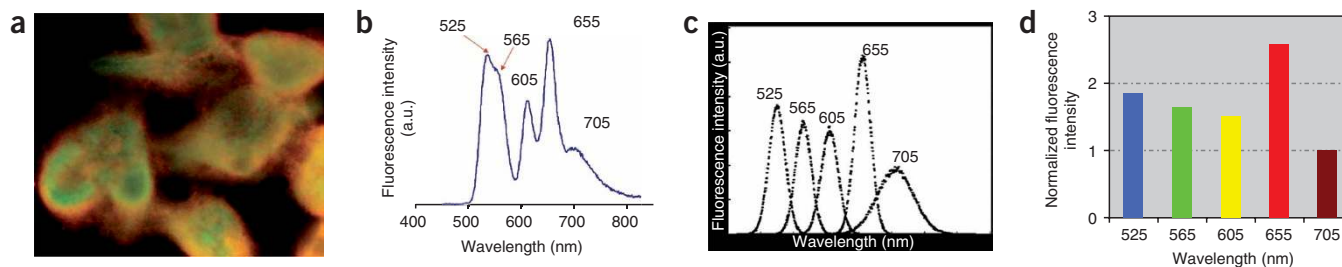


**Figure 6** | Multicolor QD staining of human prostate cancer cells, and biomarker normalization using a housekeeping gene product as the internal reference. (a) Color fluorescence image of prostate cancer cells stained with five different QDs: QD525 staining vimentin; QD565 staining N-cadherin; QD605 staining RANKL; QD655 staining E-cadherin; and QD705 staining the housekeeping gene product (elongation factor-1 $\alpha$ ). (b) Raw wavelength-resolved QD data from a QD-stained cell specimen. (c) Deconvoluted data showing the individual QD spectra. (d) Quantitative protein biomarker data as normalized by the internal reference (based on the area under each deconvoluted QD spectrum). The images are raw data from a color CCD camera.

### Step 3C

Additionally, the lack of staining or weak signal could be caused by a wrong hydrophobic barrier pen used or a wrong antigen retrieval method.

### Unsuccessful QD–antibody conjugation

Aggregate formation: too many QDs present in buffer, too much of a reagent, e.g., EDC, wrong reaction buffer (e.g., buffer at an incorrect pH or using a free-amine containing buffer in EDC coupling reactions).

Presence of competitive proteins in the antibody solution.

### Problems relating to QD staining of cell and clinical tissue specimens

No staining: unsuccessful conjugation, QDs disrupted during conjugation, antibody lost affinity during conjugation, concentration too low, incubation time too short, antigen retrieval not correct.

Too much staining: concentration too high, antigen retrieval condition too harsh.

### ANTICIPATED RESULTS

Quantitative biomarker information can be obtained by using a spectrometer attached to the fluorescence microscope. It is however very important to use a common protein such as  $\beta$ -actin or GAPDH as an ‘internal control’. That is, one of the QD–Ab conjugates should be designed to measure the product of a housekeeping gene that is expressed at relatively constant levels in all cells. As shown in **Figure 6**, this common protein can be used to normalize the biomarker data. The use of an internal control holds great promise for overcoming a number of major problems in biomarker quantification, such as differences in the probe brightness, variations in probe binding efficiency, uneven light illumination and detector responses (see **Box 2**).

The majority of available tumor specimens are archived, FFPE tissues that might be several decades old. As the clinical outcomes of these tissues are already known, these specimens are well suited for examining the relationship between molecular

## BOX 2 | SIZE TUNABLE VS COMPOSITION TUNABLE QDS

Size-tunable properties are a hallmark of semiconductor QDs and related nanostructures. The fluorescence emission spectra of ZnS-capped CdSe QDs are tuned from blue to red by changing the core particle diameter from 1.5 to 6.0 nm. Such large size changes could, however, cause problems in many applications such as multicolor cellular imaging and immunohistochemical staining, because these particles have significantly different volumes, masses and surface areas. Moreover, size-tunable CdSe QDs show considerable variations in signal brightness (measured by the absorption coefficient and fluorescence quantum yield on a particle-to-particle basis) at different emission colors. In fact, the integrated signal intensity of green QDs (525 nm emission) is 17 times lower than that of red QDs (655 nm emission) and is almost 32 times lower than that of near-infrared dots (705 nm emission) under identical experimental conditions. It is thus not surprising that many QD users have observed that the red dots are considerably brighter than the green dots. When these dots are used to quantify biomarker expressions in the same cells or tissue specimens, the results will be misleading. To overcome this problem, recent research has shown that the QD emission spectrum can also be tuned by changing the composition of the core material while keeping the size constant<sup>52–55</sup>. In particular, alloyed semiconductor QDs (cadmium selenium telluride or CdSeTe) with both homogeneous and gradient internal structures have been prepared to achieve continuous tuning of the optical properties without changing the particle size<sup>52</sup>. Remarkably, the alloyed QDs exhibit similar fluorescence quantum yields (QE = 30–60%) and spectral widths (full-width at half-maximum or FWHM = 35 nm) as the traditional core-shell dots (FWHM = 30–35 nm). This type of QD is potentially advantageous for multiplexed cell/tissue labeling because their absorption coefficients (roughly proportional to the particle volume) are similar for all different colored dots. As a result, the brightness variability between dots with different emissions can be minimized, giving a more accurate representation of the actual profiles of biomarkers in cellular and tissue samples.

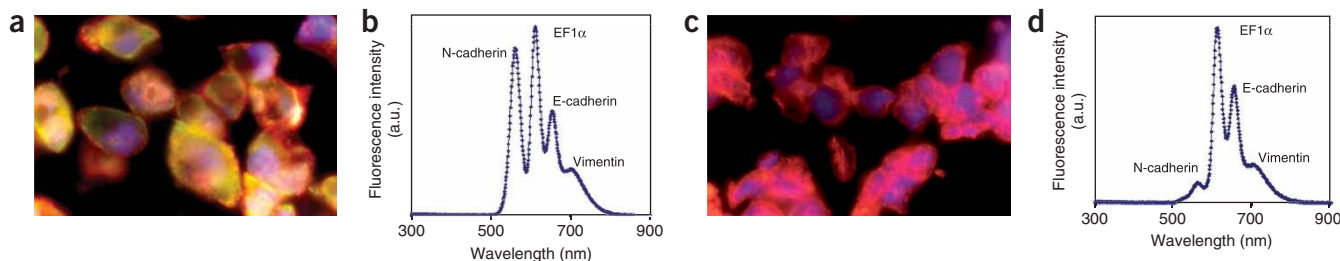


**Figure 7** | Multiplexed QD profiling of four tumor biomarkers using two FFPE prostate cancer cell lines with distinct bone-metastasis behaviors. The four markers, all associated with EMT, are N-cadherin, EF (elongation factor)-1 $\alpha$ , E-cadherin and vimentin, and their corresponding QD colors are 565, 605, 655 and 705 nm. The cell nuclei were counterstained blue by DAPI, and the QD data were captured under blue excitation. **(a)** Color fluorescence image of highly metastatic prostate cancer cells (clone ARCaPm); **(b)** single-cell QD data obtained from image **a**; **(c)** color fluorescence image of benign prostate cancer cells (clone ARCaPe); **(d)** single-cell QD data obtained from image **c**. The relative abundance of these markers is consistent with western blotting data (not shown). Note that individual cancer cells have heterogeneous expression patterns; the single-cell data in **b** and **d** are representative of a heterogeneous cell population. The images are raw data from a color CCD camera.

profile and clinical outcome in retrospective studies. One example is to study the epithelial–mesenchymal transition (EMT) process in the progression and metastasis of prostate cancer to the bone. EMT is a normal biological mechanism first reported in embryonic development and later found in cancer metastasis<sup>37</sup>. During EMT, cancer cells undergo phenotypic and behavioral changes and become more invasive, characterized by changes in the profiles of cellular adhesion molecules such as an increase of N-cadherin and a loss of E-cadherin. Other important markers for EMT include vimentin, cytokeratin 18 and RANKL. As a model system for staining optimization, we have used QD-conjugated secondary antibodies for molecular profiling of EMT using two FFPE slides from an androgen-repressed prostate cancer (ARCaP) model<sup>38</sup>. In this model, ARCaP<sub>E</sub> is more epithelial-like and less invasive, whereas the ARCaP<sub>M</sub> has more mesenchymal characteristics and is more invasive. The transition between ARCaP<sub>E</sub> and ARCaP<sub>M</sub> can be promoted by growth factors and by the interactions between prostate cancer cells and bone. Thus, this cell model represents a stepwise progression of human prostate cancer. As illustrated in **Figure 7**, we have achieved simultaneous staining of four different biomarkers with expression profiles consistent with western blot data. Moreover, QD staining provides spatial localization information (both inter- and intracellular), which is not possible with western blot or molecular biology techniques. A note of practical importance is that staining of FFPE cells requires longer incubation time (overnight at 4 °C versus 1 h at RT) and a higher QD–secondary antibody concentration than that required for freshly fixed cells.

For molecular profiling of clinical FFPE prostate specimens, we have also obtained interesting results by using four tumor antigens (mdm-2, p53, EGR-1 and p21), as shown in **Figure 8**. These markers are known to be important in prostate cancer diagnosis and are correlated with tumor behavior<sup>39,40</sup>. We are able to detect all four markers in the tissue specimens, but the autofluorescence is higher than that observed in FFPE cells. Compared with FFPE cells, clinical tissue specimens may require harsher antigen retrieval conditions (EDTA buffer vs citrate buffer) and generally have stronger autofluorescence. On the other hand, autofluorescence can be desirable by serving as a counterstain for tissue morphology. Autofluorescence can be separated from the QD signal by intentionally illuminating the sample to bleach it out while leaving the QDs bright enough for imaging and spectral analysis. Of course, spectral unmixing algorithms can be used to separate the background fluorescence from the real QD signals<sup>41,42</sup>. These early results demonstrate the feasibility of using QDs as fluorescent labels for molecular profiling of

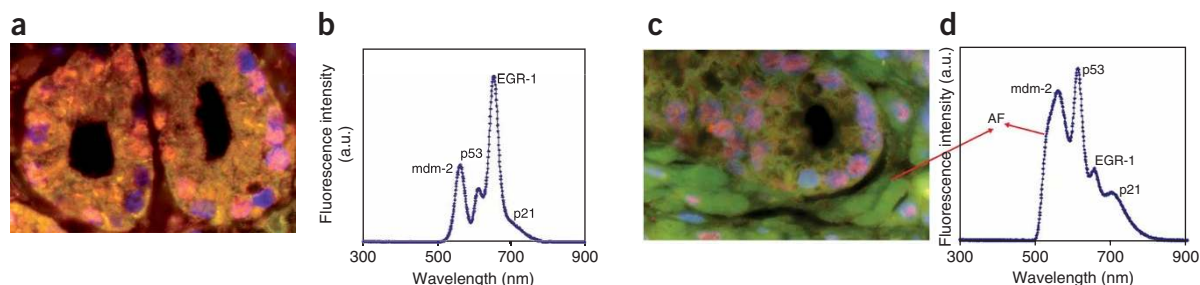


**Figure 8** | Multiplexed QD staining of archived FFPE clinical specimen from human prostate cancer patients, and comparison between two different glands on the same tissue specimen. Four tumor biomarkers (mdm-2, p53, EGR-1 and p21) were labeled with four colors of QDs emitting at 565, 605, 655 and 705 nm, respectively. **(a)** Color fluorescence image of QD-stained tissue specimens showing just one gland; **(b)** representative fluorescence spectrum obtained from single cells in the gland (image **a**); **(c)** color fluorescence image of the same QD-stained tissue specimens but showing a different gland; **(d)** representative fluorescence spectrum obtained from single cells in the second gland (image **c**). Note that the biomarker profile is remarkably different for different glands. This ability to measure cellular heterogeneity on the same tumor specimen will be crucial for clinical applications. AF stands for autofluorescence. The images are raw data from a color CCD camera.

## BOX 3 | NANOTYPING—THE USE OF MULTIPLEXED QD PROBES FOR CANCER MOLECULAR PROFILING

Significant opportunities exist at the interface between QD nanotechnology and signature biomarkers for cancer diagnosis and individualized therapy. In particular, QD nanoparticle probes can be used to quantify a panel of biomarkers on intact cancer cells and tissue specimens, allowing a correlation of traditional histopathology and molecular signatures for the same material<sup>12–14</sup>. A single nanoparticle is large enough for conjugation to multiple ligands, leading to enhanced binding affinity and exquisite specificity through a ‘multivalency’ effect. These features are especially important for the analysis of cancer biomarkers that are present at low concentrations or in small numbers of cells. Biomolecular markers are broadly defined as altered or mutant genes, RNA, proteins, lipids, carbohydrates, small metabolite molecules and altered expression of those that are correlated with a biological behavior or a clinical outcome. Most cancer biomarkers are discovered by molecular profiling studies, based on an association or correlation between a molecular signature and cancer behavior. In the cases of both breast and prostate cancer, a major progression step is the appearance of so-called ‘lethal phenotypes’ (causing patient death) such as bone metastatic, hormone independent, and radiation- and chemotherapy-resistant. It has been hypothesized that each of these aggressive behaviors or phenotypes could be understood and predicted by a defining set of biomarkers. By critically defining the interrelationships between these biomarkers, it could be possible to diagnose and determine the prognosis of a cancer based on a patient’s molecular profile, leading to personalized and predictive medicine.

FFPE clinical specimens. With continuous efforts in optimizing the experimental conditions, we believe that QD probes hold great promise in multiplexed molecular profiling of clinical tissue specimens and correlation of biomarkers with disease behavior (see **Box 3**).

It is critically important to validate the QD staining data with other available techniques. For this purpose, we have obtained QD molecular profiling data from standard human breast cell specimens, and have compared the corresponding biomarker data with traditional IHC and fluorescence *in situ* hybridization techniques. Briefly, slides from formaldehyde-fixed paraffin cell blocks were stained in accordance with standard pathological protocols for three breast cancer biomarkers—ER (estrogen receptor), PR (progesterone receptor) and HER2. This panel of protein biomarkers was selected because of its clinical significance in human breast cancer diagnosis and treatment<sup>43–46</sup>. The traditional IHC results were analyzed by two independent observers and scored with a standard scale from 0 (no visible staining in the nucleus or membrane) to 3+ (strong and complete membrane or nuclear staining in more than 10% of malignant stained cells). For a comparative analysis of QD profiling with traditional IHC, it is necessary to normalize the absolute fluorescence intensities of QD–Ab signals so that relative percentage values are calculated from the maximum signal strength.

The results reveal that a 3+ score for ER, PR or HER2 by traditional IHC corresponds to 85–100% relative expression of the antigen by QD–Ab measurement, and that 1+ or 2+ scores by traditional IHC correspond to 11–48% expression as determined by QD quantification. We note that classification of antigens expressed at low levels (1+ or 2+) is subjective, requiring experience and often resulting in considerable interobserver variations. In contrast, quantitative QD measurements allow accurate determination of tumor antigens at low levels. For example, PR expression in MCF-7 cells and ER expression in BT-474 cells are both classified as 1+ by traditional IHC, but quantitative QD measurements indicate major differences in PR expression (16.8%) and ER expression (47.7%) in these two cell lines. This indicates that the quantitative nature of QD-based molecular profiling could simplify and standardize categorization of antigens that are expressed at low levels. This is of fundamental importance in the management of breast cancer, as the likely benefit of hormonal therapies and trastuzumab depends directly on not just the presence but also the quantity of hormone or HER2 receptors<sup>47–49</sup>.

**ACKNOWLEDGMENTS** We are grateful to Dr X.H. Gao (University of Washington—Seattle) for helpful discussions, Dr R.M. Levenson (CRI, Woburn, MA) for help in spectral imaging and Dr M.W. Datta for providing human prostate cancer samples. We also acknowledge the Georgia Research Alliance (GRA) for equipment support, the Georgia Cancer Coalition (GCC) for cancer scholars awards (to S.N., M.D.W., L.W.C., and R.M.O.), Microsoft Research e-Science Funding (to M.D.W.) and the Hewlett-Packard Company for equipment support in high-speed biocomputing (to M.D.W.). The cancer nanotechnology program at Emory University and Georgia Tech is supported by a Biomedical Engineering Research Partnerships (BRP) award (R01 CA108468) and a Centers of Cancer Nanotechnology Excellence (CCNE) award (U54CA119338), both from the National Cancer Institute (NCI).

**COMPETING INTERESTS STATEMENT** The authors declare no competing financial interests.

Published online at <http://www.natureprotocols.com>  
Reprints and permissions information is available online at <http://npg.nature.com/reprintsandpermissions>

1. Bruchez, M. Jr., Moronne, M., Gin, P., Weiss, S. & Alivisatos, A.P. Semiconductor nanocrystals as fluorescent biological labels. *Science* **281**, 2013–2015 (1998).
2. Chan, W.C.W. & Nie, S.M. Quantum dot bioconjugates for ultrasensitive nonisotopic detection. *Science* **281**, 2016–2018 (1998).
3. Alivisatos, P. The use of nanocrystals in biological detection. *Nat. Biotechnol.* **22**, 47–52 (2004).
4. Pinaud, F. *et al.* Advances in fluorescence imaging with quantum dot bio-probes. *Biomaterials* **27**, 1679–1687 (2006).
5. Michalet, X. *et al.* Quantum dots for live cells, *in vivo* imaging, and diagnostics. *Science* **307**, 538–544 (2005).
6. Gao, X.H., Cui, Y.Y., Levenson, R.M., Chung, L.W.K. & Nie, S.M. *In vivo* cancer targeting and imaging with semiconductor quantum dots. *Nat. Biotechnol.* **22**, 969–976 (2004).
7. Smith, A.M., Gao, X.H. & Nie, S.M. Quantum dot nanocrystals for *in vivo* molecular and cellular imaging. *Photochem. Photobiol.* **80**, 377–385 (2004).
8. Chan, W.C.W. *et al.* Luminescent quantum dots for multiplexed biological detection and imaging. *Curr. Opin. Biotechnol.* **13**, 40–46 (2002).

9. Klostranec, J.M. & Chan, W.C.W. Quantum dots in biological and biomedical research: recent progress and present challenges. *Adv. Mater.* **18**, 1953–1964 (2006).
10. Medintz, I.L., Tetsuo-Uyeda, H., Goldman, E.R. & Mattoussi, H. Quantum dot bioconjugates for imaging, labelling and sensing. *Nat. Mater.* **4**, 435–446 (2005).
11. Chattopadhyay, P.K. *et al.* Quantum dot semiconductor nanocrystals for immunophenotyping by polychromatic flow cytometry. *Nat. Med.* **12**, 972–977 (2006).
12. Yezhelyev, M. *et al.* Emerging use of nanoparticles in diagnosis and treatment of breast cancer. *Lancet Oncol.* **7**, 657–767 (2006).
13. Xing, Y., Smith, A.M., Agrawal, A., Ruan, G. & Nie, S.M. Profiling single cancer cells and clinical tissue specimens with semiconductor quantum dots. *Int. J. Nanomed.* **1**, 473–481 (2006).
14. Gao, X.H. *et al.* In-vivo molecular and cellular imaging with quantum dots. *Curr. Opin. Biotechnol.* **16**, 63–72 (2005).
15. Wu, X.Y. *et al.* Immunofluorescent labeling of cancer marker Her2 and other cellular targets with semiconductor quantum dots. *Nat. Biotechnol.* **21**, 41–46 (2003).
16. Matsuno, A. *et al.* Three-dimensional imaging of the intracellular localization of growth hormone and prolactin and their mRNA using nanocrystal (quantum dot) and confocal laser scanning microscopy techniques. *J. Histochem. Cytochem.* **53**, 833–838 (2005).
17. Giepmans, B.N.G. *et al.* Correlated light and electron microscopic imaging of multiple endogenous proteins using quantum dots. *Nat. Methods* **2**, 743–749 (2005).
18. Ness, J.M. *et al.* Combined tyramide signal amplification and quantum dots for sensitive and photostable immunofluorescence detection. *J. Histochem. Cytochem.* **51**, 981–987 (2003).
19. Nisman, R. *et al.* Application of quantum dots as probes for correlative fluorescence, conventional, and energy-filtered transmission electron microscopy. *J. Histochem. Cytochem.* **52**, 13–18 (2004).
20. Tokumasu, F. & Dvorak, J. Development and application of quantum dots for immunocytochemistry of human erythrocytes. *J. Microsc. Oxford* **211**, 256–261 (2003).
21. Ghazani, A.A. *et al.* High throughput quantification of protein expression of cancer antigens in tissue microarray using quantum dot nanocrystals. *Nano Lett.* **6**, 2881–2886 (2006).
22. Taylor, C.R. & Levenson, R.M. Quantification of immunohistochemistry—issues concerning methods, utility and semiquantitative assessment II. *Histopathology* **49**, 411–424 (2006).
23. Guarner, J. & Zaki, S.R. Histopathology and immunohistochemistry in the diagnosis of bioterrorism agents. *J. Histochem. Cytochem.* **54**, 3–11 (2006).
24. So, M.-K., Loening, A.M., Gambhir, S.S. & Rao, J.H. Creating self-illuminating quantum dot conjugates. *Nat. Protoc.* **1**, 1160–1164 (2006).
25. Clapp, A.R., Goldman, E.R. & Mattoussi, H. Capping of CdSe–ZnS quantum dots with DHLA and subsequent conjugation with proteins. *Nat. Protocols* **1**, 1258–1266 (2006).
26. Bannai, H. *et al.* Imaging the lateral diffusion of membrane molecules with quantum dots. *Nat. Protoc.* **1**, 2628–2634 (2007).
27. Goldman, E.R. *et al.* Conjugation of luminescent quantum dots with antibodies using an engineered adaptor protein to provide new reagents for fluorimmunoassays. *Anal. Chem.* **74**, 841–847 (2002).
28. Paborsky, L.R., Dunn, K.E., Gibbs, C.S. & Dougherty, J.P. A nickel chelate microtiter plate assay for six histidine-containing proteins. *Anal. Biochem.* **234**, 60–65 (1996).
29. Jin, L. *et al.* Use of alpha-N,N-bis[carboxymethyl]lysine-modified peroxidase in immunoassays. *Anal. Biochem.* **229**, 54–60 (1995).
30. Shi, S.R., Cote, R.J. & Taylor, C.R. Antigen retrieval immunohistochemistry: past, present, and future. *J. Histochem. Cytochem.* **45**, 327–343 (1997).
31. Mortensen, E.N. & Barrett, W.A. Intelligent scissors for image composition. *Proceedings of the 22nd Annual Conference on Computer Graphics and Interactive Techniques* 191–198 (1995).
32. Hong, J.Y. & Wang, M.D. High speed processing of biomedical images using programmable GPU. *Proc. IEEE Int. Conf. Image Processing (ICIP), Singapore* 1133–1137 (2004).
33. Cormen, T.H., Leiserson, C.E., Rivest, R.L. & Stein, C. *Introduction to Algorithms* (MIT Press, Cambridge, MA, USA, 2001).
34. Weeks, A.R. & Hague, G.E. Color segmentation in the HSI color space using the K-means algorithm. *Proc. SPIE—Nonlinear Image Processing VIII* 143–154 (ACM Press, New York, USA, 1997).
35. Hermanson, G.T. *Bioconjugate Techniques* 475–478 (Academic, San Diego, CA, USA, 1996).
36. Hermanson, G.T. *Bioconjugate Techniques*, 123–124 (Academic, San Diego, CA, USA, 1996).
37. Huber, M.A., Kraut, N. & Beug, H. Molecular requirements for epithelial–mesenchymal transition during tumor progression. *Curr. Opin. Cell Biol.* **17**, 548–558 (2005).
38. Zhou, H.Y., Chang, S.M., Chen, B.Q., Wang, Y. & Zhang, H. Androgen-repressed phenotype in human prostate cancer. *Proc. Natl. Acad. Sci. USA* **93**, 15152–15157 (1996).
39. Hernandez, I. *et al.* Prostate-specific expression of p53 (R172L) differentially regulates p21, Bax, and mdm2 to inhibit prostate cancer progression and prolong survival. *Mol. Cancer Res.* **1**, 1036–1047 (2003).
40. Mora, G.R., Olivier, K.R., Mitchell, R.F., Jenkins, R.B. & Tindall, D.J. Regulation of expression of the early growth response gene-1 (EGR-1) in malignant and benign cells of the prostate. *Prostate* **63**, 198–207 (2005).
41. Mansfield, J.R., Gossage, K.W., Hoyt, C.C. & Levenson, R.M. Autofluorescence removal, multiplexing, and automated analysis methods for *in-vivo* fluorescence imaging. *J. Biomed. Opt.* **10**, 41207 (2005).
42. Levenson, R.M. Spectral imaging and pathology: seeing more. *Lab. Med.* **35**, 244–252 (2004).
43. Umemura, S. & Osamura, R.Y. Utility of immunohistochemistry in breast cancer practice. *Breast Cancer* **11**, 334–338 (2004).
44. Thomson, A. *et al.* HER-2/neu in breast cancer: interobserver variability and performance of immunohistochemistry with 4 antibodies compared with fluorescent *in situ* hybridization. *Mod. Pathol.* **14**, 1079–1086 (2001).
45. Vogel, C.L. *et al.* Efficacy and safety of trastuzumab as a single agent in first-line treatment of HER2-overexpressing metastatic breast cancer. *J. Clin. Oncol.* **20**, 719–726 (2002).
46. Elledge, R.M. *et al.* Estrogen receptor (ER) and progesterone receptor (PR), by ligand-binding assay compared with ER, PR and pS2, by immunohistochemistry in predicting response to tamoxifen in metastatic breast cancer: a Southwest Oncology Group Study. *Int. J. Cancer* **89**, 111–117 (2000).
47. Marquez, D.C. & Pietras, R.J. Membrane-associated binding sites for estrogen contribute to growth regulation of human breast cancer cells. *Oncogene* **20**, 5420–5430 (2001).
48. Hicks, D.G. & Tubbs, R.R. Assessment of the HER2 status in breast cancer by fluorescence *in situ* hybridization: a technical review with interpretive guidelines. *Hum. Pathol.* **36**, 250–261 (2005).
49. Konecny, G. *et al.* Quantitative association between HER-2/neu and steroid hormone receptors in hormone receptor-positive primary breast cancer. *J. Natl. Cancer Inst.* **95**, 142–153 (2003).
50. Matkowskyj, K.A., Schonfeld, D. & Benya, R.V. Quantitative immunohistochemistry by measuring cumulative signal strength using commercially available software Photoshop and Matlab. *J. Histochem. Cytochem.* **48**, 303–311 (2000).
51. Matkowskyj, K.A., Schonfeld, D. & Benya, R.V. Quantitative immunohistochemistry by measuring cumulative signal strength accurately measures receptor number. *J. Histochem. Cytochem.* **51**, 205–214 (2003).
52. Bailey, R.E. & Nie, S.M. Alloyed semiconductor QDs: tuning the optical properties without changing the particle size. *J. Am. Chem. Soc.* **125**, 7100–7106 (2003).
53. Jiang, W., Singhal, A., Zheng, J.N., Wang, C. & Chan, W.C.W. Optimizing the synthesis of red- to near-IR-emitting CdS-capped CdTeSe<sub>1-x</sub> alloyed quantum dots for biomedical imaging. *Chem. Mater.* **18**, 4845–4854 (2006).
54. Zhong, X.H., Han, M.Y., Dong, Z.L., White, T.J. & Knoll, W. Composition-tunable ZnxCd1-xSe nanocrystals with high luminescence and stability. *J. Am. Chem. Soc.* **125**, 8589–8594 (2003).
55. Zhong, X.H., Feng, Y.Y., Knoll, W. & Han, M.Y. Alloyed ZnxCd1-xS nanocrystals with highly narrow luminescence spectral width. *J. Am. Chem. Soc.* **125**, 13559–13563 (2003).